IEEE Access
Multidisciplinary | Rapid Review | Open Access Journal

Received 13 January 2023, accepted 7 February 2023, date of publication 10 February 2023, date of current version 15 February 2023.

Digital Object Identifier 10.1109/ACCESS.2023.3244016

RESEARCH ARTICLE

Analysis of the Speed Limit of Transrapid Maglev Train Explored From the Perspective of Its Suspension and Guidance Systems

JIE XU, XIANG YU, GUAN-CHUN LI, AND YA-JIAN LI

National Key Laboratory of Science and Technology on Vessel Intergrated Power System, Naval University of Engineering, Wuhan 430033, China
Research Department of Intergrated Power System, East Lake Laboratory, Wuhan 420202, China

Corresponding author: Jie Xu (flyinghare@126.com)

This work was supported in part by the National Natural Science Foundation of China under Grant 51825703 and Grant 51690181; and in part by the Stable Support Project of the State Administration of Science, Technology and Industry, under Grant 614221720200510.

ABSTRACT In recent years, research on high-speed or ultra-high-speed maglev systems has become increasingly popular, and different countries or teams have been committing to several different suspension technologies. Among them, due to the profound accumulation of research on the normal-conducting electromagnetic suspension technology, China is actively adopting this suspension technology to develop a new high-speed maglev train faster than 600 km/h, and this work is mainly on the basis of Transrapid (TR) trains and Shanghai Maglev Line (SHML). To evaluate the feasibility of this project, the speed limit of the TR maglev system was explored from the perspective of its suspension and guidance systems. The analysis process was carried out from two aspects of aerodynamic interference and track irregularity. As for aerodynamic interference, the aerodynamic and electromagnetic simulation models were established based on the actual maglev train. The anti-interference abilities of the suspension and guidance systems were analyzed from two aspects of steady-state and transient-state respectively. The results verified that the train could operate safely when its speed below 800 km/h and the cross-wind speed below 26 m/s. As for track irregularity, based on the actual track construction indicators of the SHML, the relationship between suspension gap fluctuation and the train speed was studied through a dynamic calculation model of the suspension control system. The results showed that the suspension system had a risk of track collision when the train speed was greater than 717 km/h. In summary, from the perspective of its suspension and guidance systems, the current TR maglev system on the SHML has an upper speed limit. The conclusion would be valuable for the development of ultra-high-speed maglev systems in the future.

INDEX TERMS Aerodynamic interference, high-speed maglev train, suspension and guidance systems, track irregularity, upper speed limit.

I. INTRODUCTION

The maglev system is characterized by contactless-type suspending support, which is very different from the traditional contact-type mechanical support, such as wheel set, sliding block, bearing and so on. Because the absence of intrinsic deficiencies of mechanical support in abrasion, noise and vibration, the maglev system has shown remarkable technical superiority and bright development prospect in the field of high-speed especially ultra high-speed applications [1]. Along with the increasing demand of people for more efficient and more convenient in transportation, quite a few researchers worldwide are keen on developing high-speed or ultra high-speed maglev systems for the past few years [2], [3], [4], [5], [6].

For developing the maglev train designed faster than 400 km/h [7], the countries who have been studying for decades and now come to the stage of technology maturity are mainly Germany and Japan. Germany started to explore the technology of normal-conducting

The associate editor coordinating the review of this manuscript and approving it for publication was Yang Tang.

This work is licensed under a Creative Commons Attribution 4.0 License. For more information, see https://creativecommons.org/licenses/by/4.0/

electromagnetic suspension (EMS) [8] from 1969 and took the first place for commercial application. In the year of 2003, China introduced the technology from Germany and built the first manned high-speed maglev commercial operation demonstration line in Shanghai [9]. However, considering the negative factors of small territory, weak demand and high cost, Germany subsequently gave up the R&D program for its Transrapid systems and stopped at TR09, whose cruising speed was designed as 505 km/h [10]. Japan adopted the technology of superconducting electrodynamic suspension (EDS) [11] to develop its high-speed maglev train from 1962, and accomplished running test on Yamanashi line with the peak speed of 603 km/h in 2015 [12], which set a new world record for the speed of ground railway trains. Now Japan is constructing a huge project of superconducting maglev operation line named Chuo Shinkansen [13], which was planned to connect the three megacities (Tokyo, Nagoya and Osaka) together to form a super metropolitan area.

As for China, in order to digest and absorb the expensive technology brought from Germany and also provide a certain degree of support for the Shanghai Maglev Line, the Ministry of Science and Technology of China (MSTC) raised fund to establish the National Maglev Transportation Engineering Technology Research Center in 2000. Some institutions were united to carry out the research of localization and innovation for the high-speed maglev train, i.e. Tongji University, National University of Defense Technology, Chinese Academy of Sciences, etc. After continuous research lasted for 15 years from the 10th to the 12th Five-Year Plan, China was able to manufacture a part of key equipment that had only been imported before and then fabricated a four-sections test train which afterwards was examined successfully on a 1.5 km maglev test line in Tongji University [14]. Nonetheless, the MSTC adjusted organization and management in the 13th Five-Year Plan and firstly encouraged a manufacturing enterprise (CRRC: China Railway Rolling Stock Corporation) to take the lead in developing 600 km/h high-speed maglev train. The CRRC integrated the related resources and accumulations over the past 15 years efficiently and manufactured a three-sections test train in May 2019. About a year later, the middle section of the test train completed a low-speed running experiment on the Tongji University 1.5 km maglev line in June 2020 [15]. However, the CRRC's test train was principally developed on the base of Transrapid SMT which is now serving on the Shanghai Maglev Line. The structural parameters of some core components (e.g. suspension, guidance and propulsion system) are almost unchanged. The Transrapid SMT was developed by Germany about 20 years ago, and its highest design speed is 500 km/h. Now, the test train made by CRRC claims that its maximum speed can reach more than 600 km/h, but its structural parameters are almost exactly the same as Transrapid SMT, only the tests of static suspension and low-speed running have been completed, so its maximum speed capacity is unconvincing. Therefore, high-speed test beyond 600 km/h is now urgently needed by CRRC.

So here is a question: how fast can the EMS type of maglev train run? In traditional view, the speed of maglev train is only relevant to its propulsion system, i.e. the pole pitch of linear motor and the current frequency of traction inverter. For this reason, CRRC increased the current frequency of the traction inverter employed for its 600 km/h test train to 355 Hz while the pole pitch of linear motor remained 258 mm. However, if one considers only from the perspective of suspension and guidance systems, does it also have a speed boundary? Hereto the authors of this article insist: as the running speed of the maglev train increases, its suspension and guidance systems will definitely be affected in three aspects, i.e. aerodynamic interference, track irregularity and vehicle-rail coupled vibration. For the third aspect, although the vibration problem is often encountered in actual experiments [16], [17], it can be solved by engineering methods, such as by use of high-rigidity and big-mass bridges; but the other two aspects would not be so easy to settle. It's because the optimization of streamline shape for the maglev train cannot greatly ameliorate its aerodynamic characteristics, e.g. aerodynamic drag reduction is lower than 10%. In addition, track accuracy is restricted by construction capacity making it difficult to improve. Therefore, this article will explore the speed limit of TR maglev train from the aspect of its suspension and guidance systems, exactly in aspects of aerodynamic interference and track irregularity.

II. AERODYNAMIC CALCULATION AND RESULT ANALYSIS

Numerical calculation of maglev train aerodynamics belongs to the category of computational fluid dynamics (CFD). Compared with various model tests or actual vehicle tests, the numerical calculation can be used for flexible comparison and selection of multiple schemes, with a shorter period and a lower cost. For this reason, we used numerical calculation to study and analyze the aerodynamic characteristics of TR maglev train above 500 km/h, which was difficult to achieve by use of other methods. The name of the software used for CFD simulation analysis is STAR-CCM+, which is a commonly used commercial hydrodynamics simulation software. But before that, some points that need special explanation are as follows:

- For the high-speed maglev train, its surrounding flow field has obvious separation characteristics, e.g. boundary layer separation, large sideslip angles, scattered wakes, etc., which requires a high-precision calculation method and a high-quality meshing.
- When the speed is greater than 500 km/h, the Mach number reaches 0.4, and the compressibility of the flow field needs to be considered.
- Because turbulence is definitely there, this calculation will utilize the κ-ε turbulence model that has been widely used in engineering.

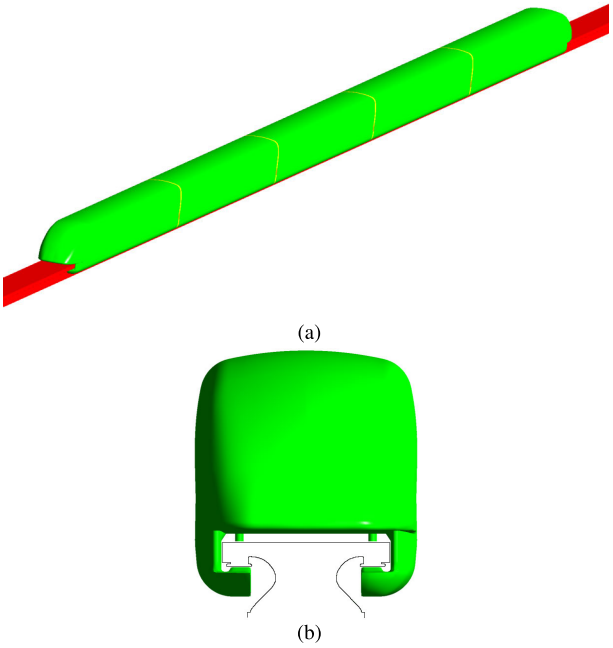

FIGURE 1. Aerodynamic calculation model of TR SMT: (a) isometric view; (b) section view.

- In view of the complexity of optimization process, non-unique goals and insignificant improvement of aerodynamic characteristics compared with current scheme, the calculation will be directly based on the existing streamline shape, which can keep a certain margin for the speed limit analysis results.

A. CALCULATION MODEL AND RELATED SETTINGS

The 1:1 manned maglev train in actual operation was used to establish the calculation model, i.e. the 5-car marshalling of Shanghai maglev train named TR SMT, as shown in Fig. 1.

This calculation used Pointwise to discretize the structural grids of the model, and a transition method from dense to sparse was adopted. It means that, from the far away of the train to the surface of the train, the grid size obtained by meshing is gradual, that is, far away from the surface of the train, the grid size is larger and sparse, but near the surface of the train, the grid size is smaller and dense. For the main calculation areas, hexahedral structure grids were used; while for some complex areas, polyhedral prism grids were used. Since the flow field near the train changes most drastically, the area with 2 times of the train's feature height was densified, and the slenderness ratio of spatial grids was controlled to be less than 2:1 to ensure the grid quality. There were 35 boundary layers on the surface of the train, and the slenderness ratio of these boundary layers was 10:1, so that enough nodes were generated in the range of viscous effect. The total number of grids in the calculation area was approximately 220 million. As an example, Fig. 2 shows the meshing result of the train head and the matching track.

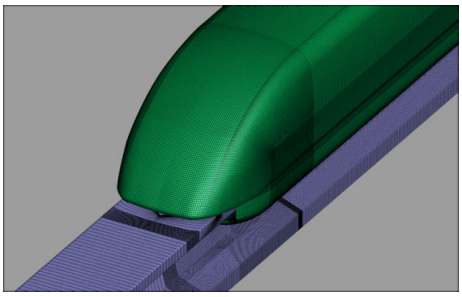

FIGURE 2. Meshing result of the train head and the matching track.

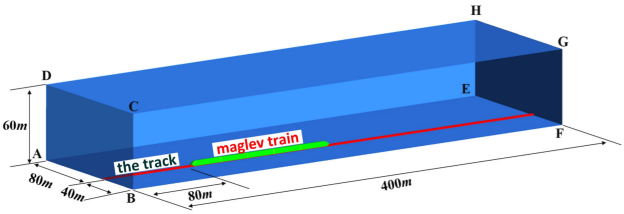

FIGURE 3. Aerodynamic calculation area and its size parameters.

TABLE 1. Size parameters of the maglev train named Transrapid SMT.

Car Categories	Length	Width	Height
Lead Car	27.5 m	3.7 m	4.66 m
Middle Car 1	24.5 m	3.7 m	4.16 m
Middle Car 2	24.5 m	3.7 m	4.16 m
Middle Car 3	24.5 m	3.7 m	4.16 m
Tail Car	27.5 m	3.7 m	4.66 m

The aerodynamic calculation area and its size parameters are shown in Fig. 3. In addition, the size parameters of the maglev train are shown in Tab. 1. The surface ABCD was defined as a pressure far field boundary, setting flow velocity by the Mach number (i.e. the train speed); while the surface EFGH was defined as a pressure outlet boundary. The train, track and ground were all defined as the boundary condition of wall; In addition, the ground was set as a sliding wall in order to reduce the influence of ground effect. Considering the generation, development and diffusion of the vortex at the tail of the train, the computational domain of the tail was longer than that of the head. The same reason also applies to the crosswinds, which all blow from B to A.

The calculation condition was in an open atmosphere environment, and the train speed was set to 500 km/h, 550 km/h, 600 km/h, 650 km/h, 700 km/h and 800 km/h respectively. In order to reduce the amount of calculation, the calculation for cross-wind impact was only carried out at the train speed of 800 km/h. Five levels of cross-wind were applied, which were 12 m/s, 15 m/s, 19 m/s, 22 m/s and 26 m/s. Due to the large model size and too many grids, the calculation process was carried out on a supercomputer named Sunway TaihuLight, which is now placed in the Wuxi city of Jiangsu province.

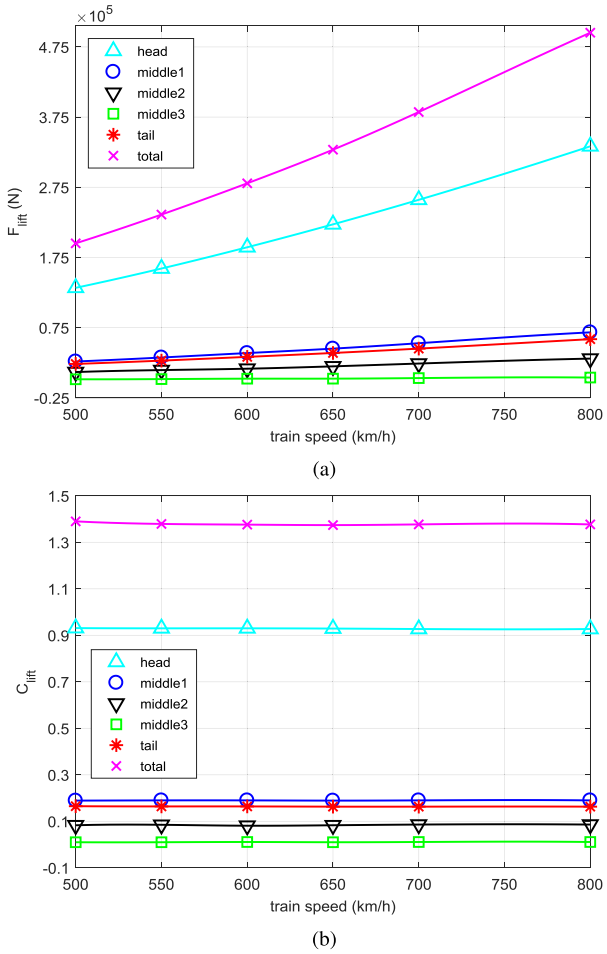

FIGURE 4. Aerodynamic lift vs train speed: (a) lift value; (b) lift coefficient.

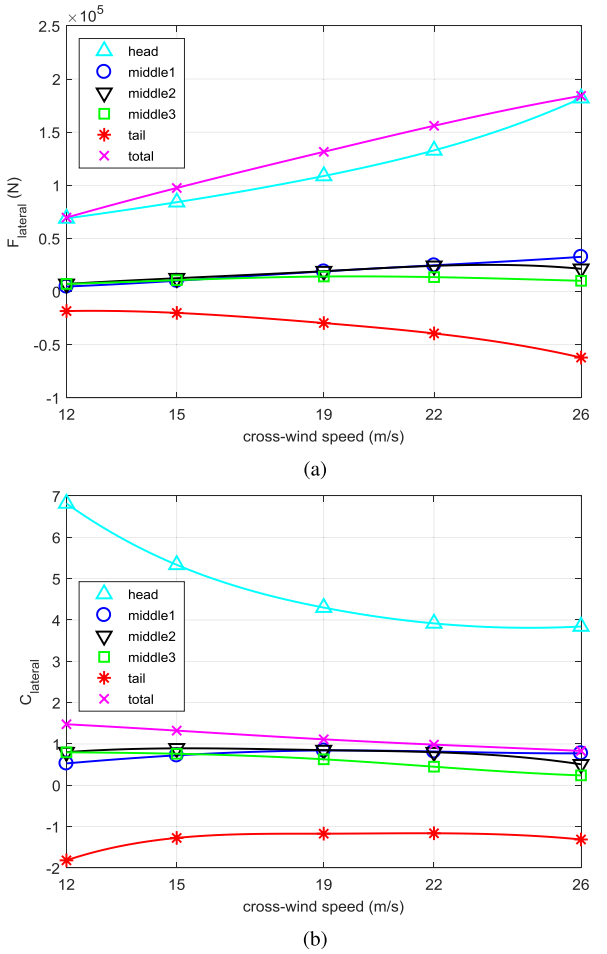

FIGURE 5. lateral force at 800 km/h vs cross-wind speed: (a) lateral force value; (b) lateral force coefficient.

B. CALCULATION RESULTS: AERODYNAMIC LIFT VS TRAIN SPEED

The aerodynamic drag and aerodynamic lift of each car of the train were calculated, but only the calculation result of aerodynamic lift versus train speed was displayed here, as shown in Fig. 4. In the figure, the dimensionless quantity C_{lift} (lift coefficient) was calculated by the formula $C_{lift} = 2F_{lift}/\rho SV^2$; Among them, ρ is the air density (1.225 kg/m^3), V is the train speed, S is the windward area (11.89 m^2).

As can be seen from Fig. 4, along with the increasing of train speed, the value of aerodynamic lift increases significantly, but the lift coefficient of each car basically remains unchanged. Compared with other cars, the aerodynamic lift of the lead car takes up a larger proportion of the whole train (about 65%); In addition, from the middle car 1 to 3, the aerodynamic lift is almost exponentially reduced. It is because the narrow gap (8-12 mm) between the train and track beams obstructs the bottom flow field. Affected by the flow field at the rear of the train, the aerodynamic lift of the tail car is greatly improved compared to the middle car 2 and 3. In short, aerodynamic lift has the greatest impact on the head car, which will be used as an object in the next analysis.

C. CALCULATION RESULTS: LATERAL FORCE VS CROSS-WIND SPEED

The aerodynamic lift, lateral force and overturning moment of each car of the train at 800 km/h were calculated. Because this article mainly focuses the impact of cross-wind on the guidance system, so only the calculation result of lateral force versus cross-wind speed was displayed here, as shown in Fig. 5. In the figure, the dimensionless quantity $C_{lateral}$ (lateral force coefficient) was calculated by the formula $C_{lateral} = 2F_{lateral}/\rho SV^2$; Among them, ρ is the air density (1.225 kg/m^3), V is the cross-wind speed, S is the windward area (end car: 114.40 m^2, middle car: 101.92 m^2, total car: 534.56 m^2).

As can be seen from Fig. 5, along with the increasing of cross-wind speed, the value of lateral force increase significantly, especially for the lead car and the tail car. In particular, due to the simultaneous effects of wake and cross-wind, the lateral force direction of the tail car is opposite to that of other cars. However, the lateral force of the whole train still increases significantly with the increasing of cross-wind speed. When the cross-wind speed increases from 12 m/s to 26 m/s, the lateral force of the whole train increases from

about 70 *kN* to 184 *kN*. However, unlike the lift coefficients in Fig. 4(b), the lateral force coefficient of each car no longer maintains an approximate constant value, especially for the lead car. The reason may be that, the wind direction in the simulation model is no longer unique at this time, including the vehicle speed of 800 km/h and a relatively small cross-wind, and the calculation result of lateral force is obtained under the combined action of the vehicle speed and the cross-wind. Therefore, it is inaccurate to calculate the lateral force coefficient only by substituting the cross-wind into the empirical formula. However, Fig. 5(b) still reflects some important information. For example, the change in the lateral force coefficients of the middle car and the total car is very small, namely cross-winds have a greater impact on the lead car of a maglev train under ultra-high-speed operating conditions.

III. ANALYSIS OF THE INFLUENCE OF AERODYNAMIC INTERFERENCE

One can see from Section II: as the train speed increases, the aerodynamic lift continues to increase and will affect the suspension system, which is a steady-state static analysis; while the impact of cross-wind at high speed will affect the guidance system, which is a transient dynamic analysis. This section will discuss from these two aspects. In this regard, it is necessary to say a few more words. Considering the ride comfort of passengers, the acceleration of the maglev train is very small, generally less than 0.1 g. In a long acceleration time, the change of aerodynamic lift caused by the train motion is a very slow process, so the influence of aerodynamic lift on the suspension system can be regarded as a steady-state static analysis. However, cross-winds are usually accidental, so the influence of cross-winds on the train guidance system can be regarded as a transient dynamic analysis.

The lead car and the tail car (hereinafter collectively referred as the end cars) of TR SMT have an empty load of 52.9 *tons* and a full load of 67 *tons*; Each middle car has an empty load of 50.3 *tons* and a full load of 69.5 *tons*. No matter the end car or the middle car, they are suspended and guided by several electromagnet modules, as shown in Fig. 6. If calculated equivalently, each end car includes 15 suspension electromagnet modules and 12 guidance electromagnet modules; Each middle car includes 16 suspension electromagnet modules and 12 guidance electromagnet modules.

A. AERODYNAMIC LIFT ON THE SUSPENSION SYSTEM

The structural dimensions and electrical parameters of a single suspension electromagnet module are shown in Tab. 2. Based on this table and the three-dimensional model shown in Fig. 6, a finite element electromagnetic simulation model of the suspension electromagnet module was established, as shown in Fig. 7(a). In the model, the stator and iron-core pole are made of laminated silicon steel material, and the iron-core yoke is made of solid iron material. The windings and suspension coils are both made of aluminum wires. The software used for the electromagnetic analysis is ANSYS Electromagnetics Suite, which uses the finite element method

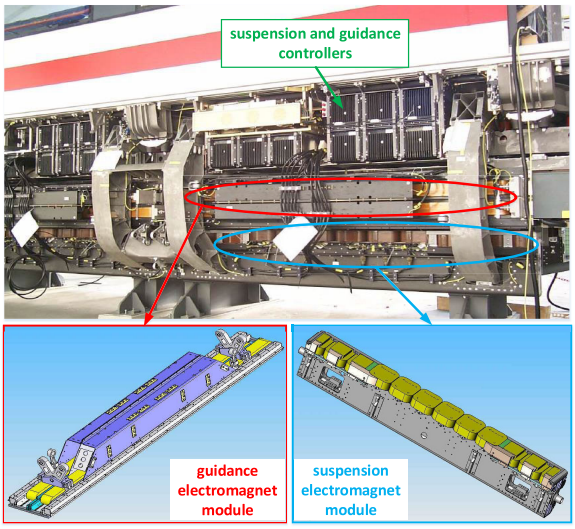

FIGURE 6. Suspension and guidance electromagnet modules and their controllers.

TABLE 2. Structural dimensions and electrical parameters of a single suspension electromagnet module.

Polar Length (middle pole)	pl_m	170 mm
Polar Length (end pole)	pl_e	85 mm
Polar Width	pw	168 mm
Pole Height (middle pole)	ph_m	146 mm
Pole Height (end pole)	ph_e	174 mm
Pole Distance	pd	266.5 mm
Rated Suspension Gap	rg	10 mm
Number of Turns Per Coil	nc	270
Coil Material	—	Aluminum

to analyze the problem of static magnetic field, and the boundary condition was set as Vector Potential Boundary. After simulation and calculation, the relationship between the suspension force generated by a single suspension electromagnet module and the coil current is shown in Fig. 7(b).

As can be seen from Fig. 7(b), when the coil current reaches about 40 A, the suspension force curve begins to enter the ''knee point''. After that, the nonlinearity is enhanced, which is not conducive to the implementation of commonly used linear control algorithms. The same is true when the coil current is less than 10 A. Therefore, 10 A to 40 A can be roughly regarded as the regional boundary of the rated coil current.

In actual operation, the acceleration of TR maglev train is generally less than 0.15 g, i.e. the time required for the train to accelerate from standstill to a high-speed state above 500 km/h is at least 95 s. This is a low bandwidth for the suspension control system and can be regarded as a steady-state transformation. In addition, load change only occurs when the train stops and passengers get on or off, which is completely a steady-state mechanical analysis. Combining the calculation results of aerodynamic lift in Fig. 4, the results

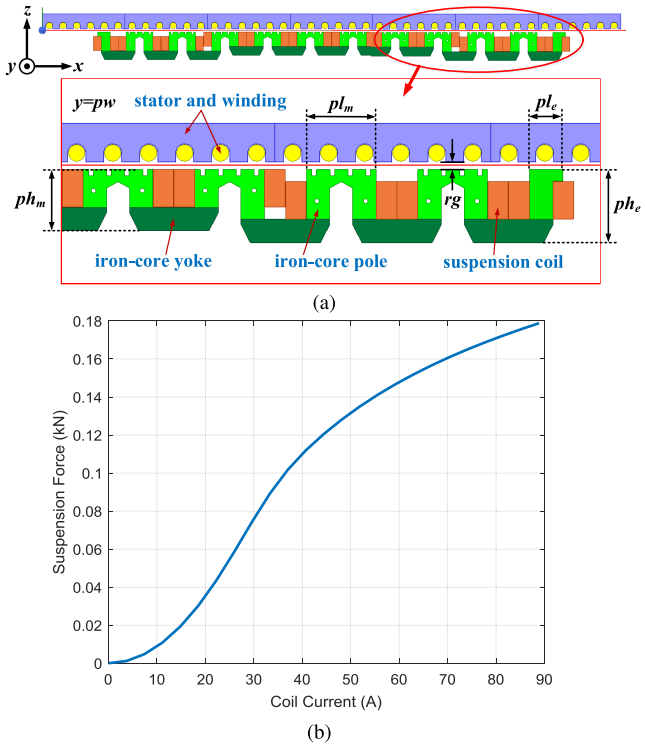

FIGURE 7. Electromagnetic simulation of the suspension electromagnet module: (a) simulation model; (b) suspension force vs coil current.

TABLE 3. Steady-state suspension current of each car at 800 km/h.

Car Categories	Empty Load	Full Load
Lead Car	11.7 A	14.3 A
Middle Car 1	17.3 A	19.9 A
Middle Car 2	18.1 A	20.6 A
Middle Car 3	18.6 A	21.1 A
Tail Car	18.6 A	20.3 A

of electromagnetic simulation in Fig. 7 and the train load changes, the steady-state suspension current of each car at 800 km/h (the most severe working condition) is shown in Tab. 3.

As can be seen from Tab. 3, since there are many suspension electromagnet modules installed on each car, the current fluctuation caused by aerodynamic lift and load changes in each electromagnet module is 11.7 A to 21.1 A, which is within the range of linear control algorithm (10 A to 40 A). That is, when the train speed is below 800 km/h, the influence of aerodynamic lift on the suspension system is controllable.

B. CROSS-WIND IMPACT ON THE GUIDANCE SYSTEM

The technical parameters, simulation model and force-current curve of a single guidance electromagnet module are shown in Tab. 4, Fig. 8(a) and Fig. 8(b), respectively.

It can be seen from Fig. 8(b), 10 A to 80 A can be roughly regarded as the regional boundary of the rated coil current in the guidance electromagnet. The specific reason is similar to

TABLE 4. Structural dimensions and electrical parameters of a single guidance electromagnet module.

Polar Length	pl	800 mm
Polar Width	pw	28 mm
Window Width	ww	94 mm
Window Height	wh	40 mm
Yoke Thickness	yt	24 mm
Rated Guidance Gap	rg	10 mm
Number of Turns Per Coil	nc	200
Coil Material	—	Aluminum

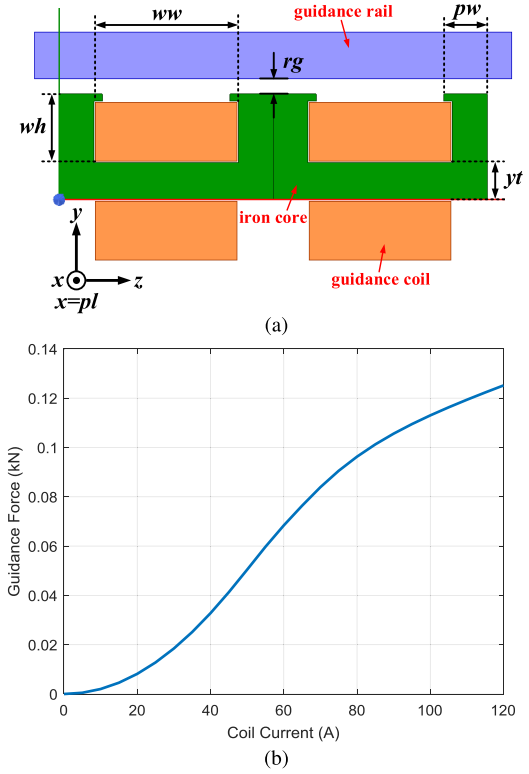

FIGURE 8. Electromagnetic simulation of the guidance electromagnet module: (a) simulation model; (b) guidance force vs coil current.

that of the suspension electromagnet. However, for transient conditions this boundary can be expanded appropriately.

When a cross-wind occurs, it is equivalent to a transient impact loaded on the guidance system. At this time, the guidance electromagnets on both sides of the train adopt a differential working mode, i.e. the coil current in the electromagnets on one side increases while the coil current in the electromagnets on the other side reduces, then a differential force is generated to resist the impact of cross-wind. As shown in Fig. 5(a), the lead car bears the largest lateral force at 800 km/h, reaching 182 kN at the cross-wind speed of 26 m/s, and this force will be mainly borne by 6 guidance electromagnets on one side.

A dynamic simulation model of the guidance system was established in Matlab/Simulink, the model included a differential guidance controller, which was based on the commonly

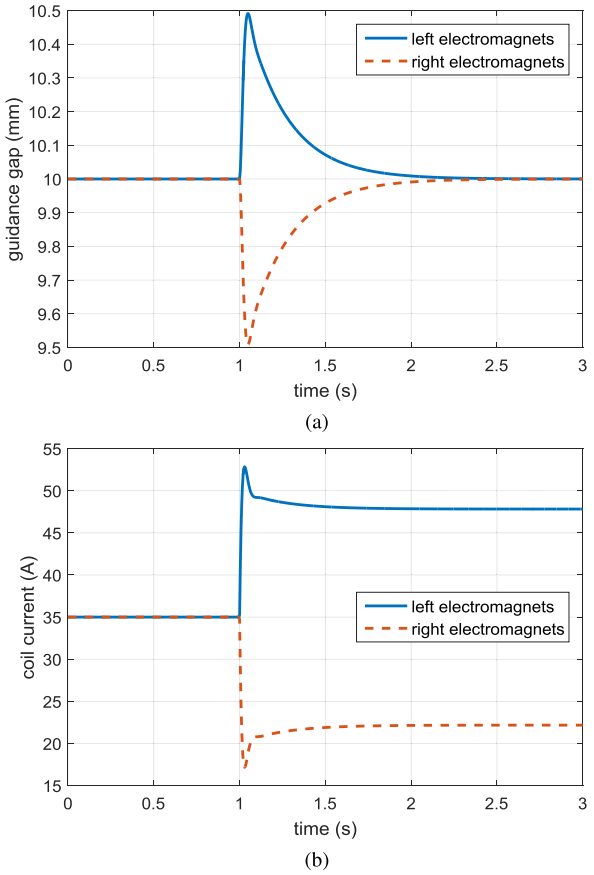

FIGURE 9. Dynamic simulation of the guidance system suffering cross-wind at the train speed of 800 km/h: (a) guidance gap; (b) coil current.

used PID algorithm. The simulation settings were as follows: 1) the train speed was 800 km/h; 2) the fixed step was 50 μs and the total time was 3 s; 3) the lateral force of 182 kN produced by the cross-wind speed of 26 m/s (supposing it blew from the right side) was added as a step disturbance at 1 s. The curves of guidance gap and coil current obtained by simulation were shown in Fig. 9(a) and Fig. 9(b), respectively.

As can be seen from Fig. 9, when the running train suddenly encounters a cross-wind, the guidance system can respond in time under the action of its controller and restore the system to its original state in about 1 s. In this process, the maximum fluctuation of guidance gap on both sides relative to the steady-state gap value 10 mm is less than 0.5 mm. Simultaneously, the variation of the coil current in the electromagnets on both sides is between 14-54 A, which is within the actuating range of linear control algorithm (10 A to 80 A). That is, when the train speed is below 800 km/h, the influence of cross-wind on the guidance system is controllable.

C. SUMMARY OF THIS SECTION

Based on the results of aerodynamic calculation and analysis in Section II, this section analyzed the anti-interference ability of the suspension and guidance systems of TR maglev train from two aspects of steady-state and transient-state respectively. The results show that the train can work safely at speeds below 800 km/h. It means, if only considering in aspect of aerodynamic, the speed limit of electromagnetic suspension and guidance system is not lower than 800 km/h.

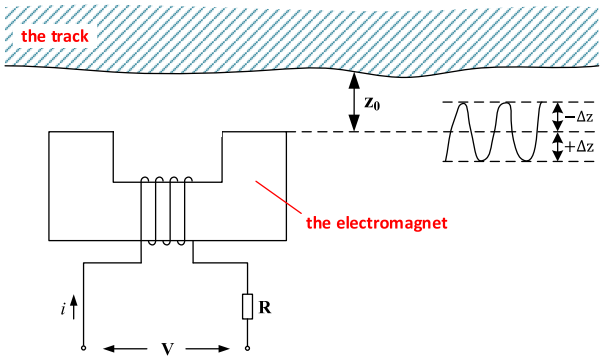

FIGURE 10. Principle and structure diagram of track irregularity.

IV. ANALYSIS OF THE INFLUENCE OF TRACK IRREGULARITY

A. PREFACE OF THIS SECTION

The EMS type suspension system adjusts the state of its electromagnet in real time through the controller to ensure that the rated suspension gap z_0 is maintained between the electromagnet and the track. Therefore, the suspension control essentially belongs to the tracking problem of the electromagnet to the track. When the track changes beyond the tracking ability of the suspension system, the suspension gap will produce fluctuations Δz. According to our long-term engineering experience in the commissioning of maglev trains, a general conclusion considering operational safety is summarized that when $\Delta z > (1/3)z_0$, the electromagnet has the risk of hitting the track. So, this inequality is usually used as a criterion for suspension failure. The Principle and structure diagram of track irregularity is shown in Fig. 10.

The maglev train is a large inertial system with a low bandwidth. It can better track low-frequency changes in the track (i.e. long-wave irregularities), but high-frequency changes (i.e. short-wave irregularities) will cause suspension fluctuations. However, as the train speed increases, low-frequency and long-wave irregularities may become high-frequency and short-wave irregularities, which for the suspension system means that the track irregularities are aggravated, thereby affecting the stability of the system. In theory, if the track is absolutely straight, there is no speed limit for the suspension system. However, deformation, settlement and installation errors of some structural parts in actual engineering will cause track irregularities. Therefore, the analysis will take the actual track irregularity data of the TR maglev system as input and bring it into a dynamic calculation model to obtain the

suspension gap fluctuation at different train speeds, and then deduct the speed limit of the suspension system.

It is worth pointing out that, the purpose of this section is to qualitatively explain whether track irregularity will affect the speed capability of TR maglev train from the perspective of its suspension or guidance system, rather than deliberately calculating and obtaining an exact upper limit of speed. Therefore, limited by the length of the text and the lack of relevant data, in this section we will only take the suspension system as an example to illustrate the simulation method of calculation and analysis. This method is also suitable for the guidance system with the same working principle, it is just that the indicator of guidance track irregularities may get a different result value, but this specific value is not the focus of this section.

B. TYPES AND INDICATORS OF THE ACTUAL TRACK IRREGULARITIES

The TR maglev train runs on an elevated line, as shown in Fig. 11(a). Except for some special sections, the span of the elevated track beam is a standard length 24.8 m. Functional parts made of steel are installed on the track beams to fix some functional surfaces, including the lower stator surface, the side guidance surface and the top sliding surface, as shown in Fig. 11(b). Similarly, the functional parts are 3.1 m in standard length.

Since the track beams and the functional parts are of standard length, the track irregularities caused by the following factors can be approximately regarded as periodic: 1) deformation and settlement of the track beams; 2) installation misalignment and deviation of the functional parts. The schematic diagram of these types of periodic track irregularities is shown in Fig. 12.

The deformation of track beams mainly refers to the static deflection caused by the increasing load when the train passes, and its irregularity can be approximated by the following formula (where $x = Vt$, representing the distance travelled by the train):

$$y_1 = -a_1|sin(\pi \frac{x}{L_a})|; x_{period} = L_a \tag{1}$$

Similarly, the settlement of track beams and the installation misalignment and deviation of functional parts can be described by the following three formulas respectively:

$$y_2 = -a_2(1 - |\frac{x}{L_a}|), |x| \le L_a; x_{period} = 2L_a \tag{2}$$

$$y_3 = \begin{cases} 0, & -L_b \le x \le 0 \\ b_1, & 0 < x \le L_b \end{cases}; x_{period} = 2L_b \tag{3}$$

$$y_4 = b_2(1 - |\frac{x}{L_b}|), |x| \le L_b; x_{period} = 2L_b \tag{4}$$

Corresponding to the classification described above, the track irregularities of the Shanghai Maglev Line are listed as follows [18]:

(a)

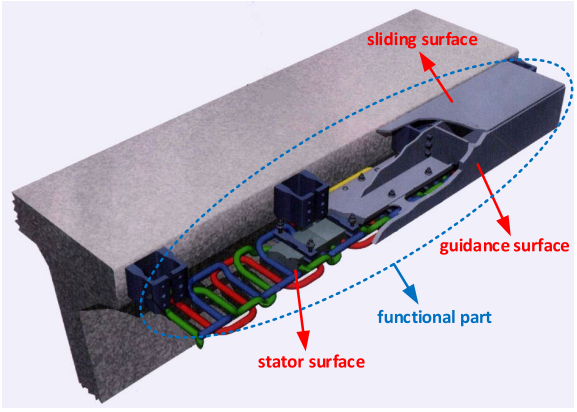

(b)

FIGURE 11. Track beam and functional part of the TR maglev train: (a) track beam; (b) functional part.

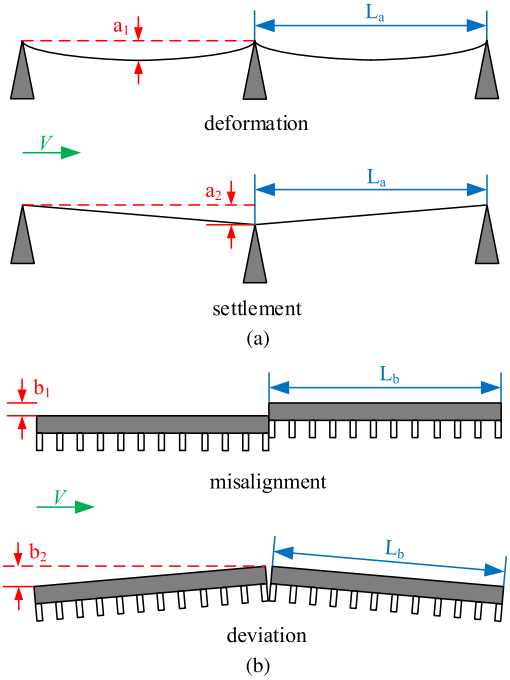

FIGURE 12. Schematic diagram of several types of periodic track irregularities: (a) track beam; (b) functional part.

- The deformation of track beams needs to be controlled within $L_a/4800$. For the track beam of 24.8 m, it means $a_1 = 5.17\ mm$.

TABLE 5. Main parameters and their values used in the dynamic calculation model.

Mass of a Middle Car	G	50.3 $tons$
Number of Equivalent Single-electromagnets	n	176
Load of a Single-electromagnet	m	286 kg
Acceleration of Gravity	g	9.8 m/s^2
Vacuum Permeability	μ_0	1.257e-6 H/m
Number of Turns Per Coil	N	270
Resistance of a Single Coil	R	1.5 Ω
Pole Area of a Single-electromagnet	S	0.0143 m^2
Rated Suspension Current	i_0	29 A
Rated Suspension Gap	z_0	10 mm
Control Frequency	f	4 kHz
Chopper Voltage Limit	U_L	440 V
Coil Current Limit	I_L	150 A

- The settlement of track beams needs to be controlled within L_a/6000. For the track beam of 24.8 m, it means $a_2 = 4.13$ mm.
- The maximum allowable installation misalignment of functional parts $b_1 = 0.6$ mm.
- The maximum allowable installation deviation of functional parts $b_2 = 1.5$ mm.

C. MODELING CALCULATION AND RESULT ANALYSIS

Based on the technical parameters of the suspension electromagnet and the maglev train in Section III, we established a dynamic calculation model of the suspension control system. The main parameters and their values used in the model are shown in Tab. 5.

In addition, the main calculation formulas related to the model are shown in the following equations [14], [19], [20], in which Eqn. (5)-(7) and Eqn. (8)-(12) refer to electrical equations and mechanical equations respectively.

$$L = \frac{\mu_0 N^2 S}{2z} \tag{5}$$

$$M = \frac{\mu_0 N^2 S i}{2z^2} \tag{6}$$

$$U = Ri + L\frac{di}{dt} + M\frac{dz}{dt} \tag{7}$$

$$z = z_m - z_t \tag{8}$$

$$F = \frac{\mu_0 N^2 S i^2}{4z^2} = mg + ma_m \tag{9}$$

$$v_m = \int_0^t a_m dt \tag{10}$$

$$z_m = \int_0^t v_m dt \tag{11}$$

$$z_t = y_1 + y_2 + y_3 + y_4 \tag{12}$$

In the above equations from Eqn. (5)-(12), the description of some letter symbols which has not been defined before is shown in Tab. 6.

The tracking and robustness of the system were comprehensively considered, and the fluctuations of suspension gap caused by track irregularities at high speeds were minimized as much as possible. After debugging, the control system parameters were determined as: 1) Inner-loop parameter for suspension current k_c=200; 2) Outer-loop parameters for suspension gap k_p=7500, k_i=10 and k_d=250. These parameters are very close to those used in many actual maglev systems.

TABLE 6. Supplementary description of the letter symbols in the dynamic equations.

L	Self-inductance of a Single Coil
M	Inter-inductance of Electromagnet Coils
U	Voltage Across Electromagnet Coils
F	Real-time Suspension Force
i	Real-time Suspension Current
z	Real-time Suspension Gap
z_m	Position of the Electromagnet
a_m	Acceleration of the Electromagnet
v_m	Velocity of the Electromagnet
z_t	Position of the Track

The actual indicators of track irregularity mentioned above were introduced into the model and the corresponding result was obtained. The simulation was divided into two cases: 1) Only the settlement of the track beams with the largest amplitude of track irregularity was firstly considered; 2) Four types of track irregularities were simultaneously considered. As the train speed increases, the situations of suspension gap z and its fluctuation Δz relative to the rated value $z_0 = 10mm$ are shown in Fig. 13.

As shown in Fig. 13(a), the fluctuations of suspension gap increase rapidly with the increasing of train speeds. When the train speed reaches 786 km/h for case 1 and 717 km/h for case 2 respectively, the fluctuations of suspension gap exceed 1/3 of the rated gap, which is about 3.33 mm. According to the criteria mentioned above, it can be considered that the bearing capacity of suspension system has reached the limit under these circumstance.

Fig. 13(b) and Fig. 13(c) severally show the dynamic curves of suspension gap at the train speeds of 786 km/h for case 1 and 717 km/h for case 2, in which the track irregularities were added at 25 s and removed at 75 s. The curves show that the fluctuation frequencies of suspension gap are about 8-9 Hz. Because it is a low frequency, the suspension system has to choose tracking, which is the essential reason that restricts the speed limit of suspension system.

However, in the actual system, not all track irregularities appear at the same time with their maximum limits. In other words, the simulation in this section is actually the most severe situation. In addition, the track irregularity index of high-speed maglev systems can be further improved within the range allowed by construction cost, so the speed capacity of TR maglev trains can also be improved to a certain extent. However, as analyzed and obtained in this section, there will still be a boundary.

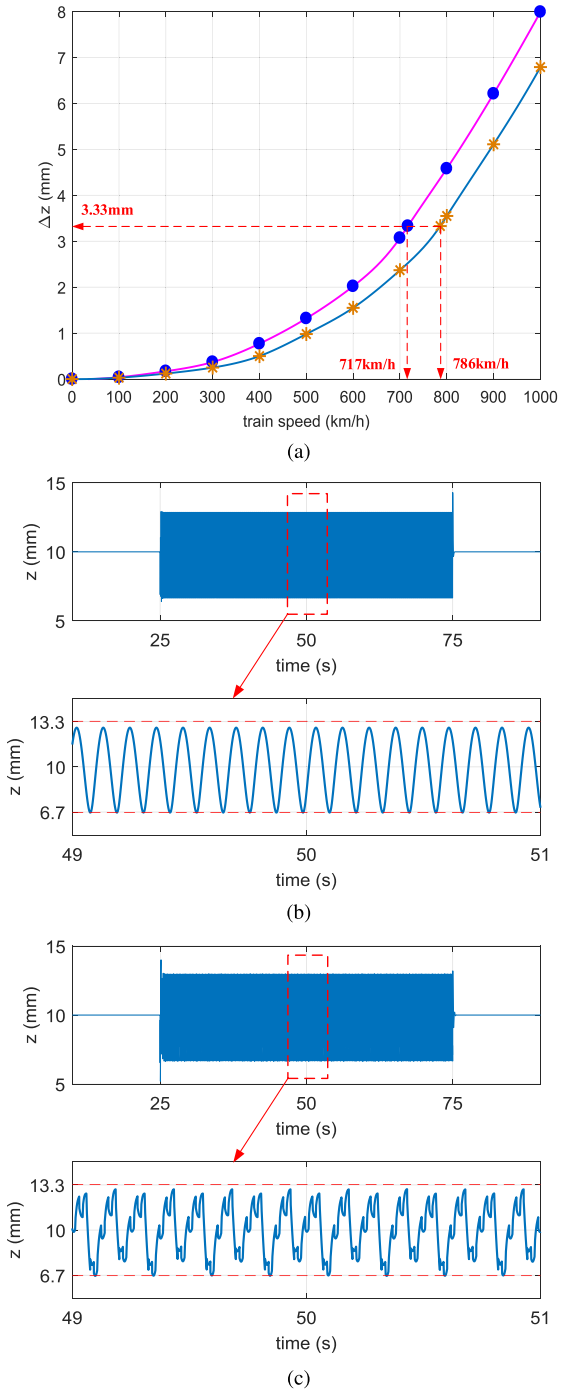

FIGURE 13. Suspension gap and its fluctuation: (a) gap fluctuation vs train speed; (b) gap curve at 786 km/h for case 1; (c) gap curve at 717 km/h for case 2.

V. CONCLUSION

The TR maglev train used the mature EMS-type suspension technology and has achieved a peak speed of 501 km/h in the test of Shanghai Maglev Line. At present, China is using this technology to build a new high-speed maglev train faster than 600 km/h. To evaluate the feasibility of this project, the speed limit of the TR maglev system was explored. We believe the speed limit of a maglev train is not only related to its propulsion system; For the EMS-type maglev train that has a small air gap and relies on active control system, aerodynamic interference and track irregularity at high speed will have a non-negligible impact on its suspension and guidance systems.

As for aerodynamic interference, the aerodynamic and electromagnetic simulation models were established based on the actual maglev train. The anti-interference abilities of the suspension and guidance systems were analyzed from two aspects of steady-state and transient-state respectively. The results verified that the train could operate safely when its speed below 800 km/h and the cross-wind speed below 26 m/s. As for track irregularity, based on the actual track construction indicators of the Shanghai Maglev Line, we studied the relationship between suspension gap fluctuation and the train speed through a dynamic calculation model of the suspension control system. The results showed that the suspension system had a risk of track collision when the train speed was greater than 717 km/h.

In summary, from the perspective of its suspension and guidance systems, the current TR maglev system in Shanghai has an upper speed limit. We hope this conclusion could give some enlightenment for the development of ultra-high-speed maglev systems in the future.

REFERENCES

[1] H.-W. Lee, K.-C. Kim, and J. Lee, "Review of Maglev train technologies," *IEEE Trans. Magn.*, vol. 42, no. 7, pp. 1917–1925, Jul. 2006.
[2] P. E. Ross, "Hyperloop: No pressure," *IEEE Spectr.*, vol. 53, no. 1, pp. 51–54, Jan. 2016.
[3] J. Braun, J. Sousa, and C. Pekardan, "Aerodynamic design and analysis of the hyperloop," *AIAA J.*, vol. 55, no. 12, pp. 4053–4060, Dec. 2017.
[4] A. S. Abdelrahman, J. Sayeed, and M. Z. Youssef, "Hyperloop transportation system: Analysis, design, control, and implementation," *IEEE Trans. Ind. Electron.*, vol. 65, no. 9, pp. 7427–7436, Sep. 2018.
[5] W.-Y. Ji, G. Jeong, C.-B. Park, I.-H. Jo, and H.-W. Lee, "A study of non-symmetric double-sided linear induction motor for hyperloop all-in-one system (propulsion, levitation, and guidance)," *IEEE Trans. Magn.*, vol. 54, no. 11, pp. 1–4, Nov. 2018.
[6] C.-Y. Lee, J.-H. Lee, J. Lim, S. Choi, J.-M. Jo, K.-S. Lee, Y. D. Chung, S. Kim, and H. Lee, "Design and evaluation of prototype high-T_c superconducting linear synchronous motor for high-speed transportation," *IEEE Trans. Appl. Supercond.*, vol. 30, no. 4, pp. 1–5, Jun. 2020.
[7] A. Cassat and M. Jufer, "MAGLEV projects technology aspects and choices," *IEEE Trans. Appl. Supercond.*, vol. 12, no. 1, pp. 915–925, Mar. 2002.
[8] J. Meins, L. Miller, and W. Mayer, "The high speed Maglev transport system TRANSRAPID," *IEEE Trans. Magn.*, vol. MAG-24, no. 2, pp. 808–811, Mar. 1988.
[9] L. Yan, "Development and application of the Maglev transportation system," *IEEE Trans. Appl. Supercond.*, vol. 18, no. 2, pp. 92–99, Jun. 2008.
[10] [Online]. Available: https://www.maglev.net/transrapid-design-history
[11] M. Ono, S. Koga, and H. Ohtsuki, "Japan's superconducting maglev train," *IEEE Instrum. Meas. Mag.*, vol. 5, no. 1, pp. 9–15, Mar. 2002.
[12] [Online]. Available: http://www.bbc.com/news/world-asia-32391020
[13] K. Sawada, "Outlook of Maglev Chuo Shinkansen," in *Proc. 22th Int. Conf. Magn. Levitated Syst. Linear Drives (MAGLEV)*, 2014.
[14] Z. Liu, Z. Long, and X. Li, *Maglev Trains: Key Underlying Technologies*. Heidelberg, Germany: Springer, 2015.
[15] [Online]. Available: https://en.tongji.edu.cn/info/1009/4225.htm
[16] L. Zhang, Z. Zhang, and L. Huang, "Hybrid non-linear differentiator design for a permanent-electro magnetic suspension Maglev system," *IET Signal Process.*, vol. 6, no. 6, pp. 559–567, Aug. 2012.

[17] Z. Zhang and L. Zhang, "Hopf bifurcation of time-delayed feedback control for maglev system with flexible guideway," *Appl. Math. Comput.*, vol. 219, no. 11, pp. 6106–6112, Feb. 2013.
[18] X. Wu, *Maglev Train*. Shanghai, China: Shanghai Publisher of Science and Technology, 2003.
[19] Y.-G. Li and W.-S. Chang, "Cascade control of an EMS Maglev vehicle's levitation control system," *Acta Autom. Sinica*, vol. 25, no. 2, pp. 247–251, Mar. 1999.
[20] H.-S. Han and D.-S. Kim, *Magnetic Levitation: Maglev Technology and Applications*. Heidelberg, Germany: Springer, 2016.

JIE XU was born in Suzhou, China, in 1987. He received the B.S. degree in mechatronic engineering from Zhejiang University, Zhejiang, China, in 2010, and the Ph.D. degree in control science and engineering from the National University of Defense Technology, Changsha, China, in 2016. From 2014 to 2015, he was a Doctoral Student jointly trained with the Jülich Research Center, Germany. Since 2017, he has been an Assistant Researcher with the National Key Laboratory of Science and Technology on Vessel Intergrated Power System, Naval University of Engineering. Since 2021, he has been a part-time Researcher with the Research Department of Intergrated Power System, East Lake Laboratory. His research interests include magnetic levitation technology and applied superconductivity.

XIANG YU was born in Suizhou, China, in 1988. He received the B.S. degree in aircraft system and engineering and the M.S. and Ph.D. degrees in aeronautical and astronautical science and technology from the National University of Defense Technology, Changsha, China, in 2010, 2012, and 2017, respectively. Since 2018, he has been an Assistant Researcher with the National Key Laboratory of Science and Technology on Vessel Intergrated Power System, Naval University of Engineering. Since 2021, he has been a part-time Researcher with the Research Department of Intergrated Power System, East Lake Laboratory. His research interests include magnetic levitation control and high-performance motor control.

GUAN-CHUN LI was born in Zhumadian, China, in 1989. He received the B.S. degree in automation from Donghua University, Shanghai, China, in 2011, and the Ph.D. degree in control science and engineering from the National University of Defense Technology, Changsha, China, in 2018. Since 2018, he has been an Assistant Researcher with the National Key Laboratory of Science and Technology on Vessel Intergrated Power System, Naval University of Engineering. Since 2021, he has been a part-time Researcher with the Research Department of Intergrated Power System, East Lake Laboratory. His research interests include electric propulsion and magnetic levitation technology.

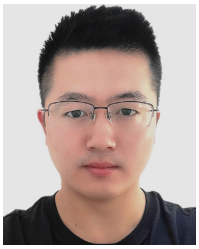

YA-JIAN LI was born in Yiyang, China, in 1990. He received the B.S. degree in automation and the M.S. and Ph.D. degrees in control science and engineering from the National University of Defense Technology, Changsha, China, in 2013, 2016, and 2020, respectively. Since 2021, he has been an Assistant Researcher with the National Key Laboratory of Science and Technology on Vessel Intergrated Power System, Naval University of Engineering. Since 2021, he has been a part-time Researcher with the Research Department of Intergrated Power System, East Lake Laboratory. His research interests include magnetic levitation control and vehicle-bridge-track coupled vibration.